Large-scale structures of scalar and velocity in a turbulent jet flow

Jesse Reijtenbagh, Jerry Westerweel, and Willem van de Water[*]
Laboratory for Aero and Hydrodynamics, Delft University of Technology
and J.M. Burgers Centre for Fluid Dynamics, 2628 CD Delft, The Netherlands

We study the relation between large-scale structures in the concentration field with those in the velocity field in a dye-seeded turbulent jet. The scalar concentration in a plane is measured using laser-induced fluorescence. Uniform concentration zones of an advected scalar are indentified using cluster analysis. We simultaneously measure the two-dimensional velocity field using particle image velocimetry. The structures in the velocity field are characterized by finite-time Lyapunov exponents. The measurement of the scalar- and velocity fields moves with the mean flow. In this moving frame, turbulent structures remain in focus long enough to observe well-defined ridges of the finite-time Lyapunov field. This field gauges the rate of point separation along Lagrangian trajectories; it was measured both for future and past times since the instant of observation. The edges of uniform concentration zones are correlated with the ridges of the past-time Lyapunov field, but not with those of the future-time Lyapunov field. We quantify this relation using both conditional averages and the ordinary correlation function.

I. INTRODUCTION

Turbulent mixing of a passive scalar in a fluid is caused by the incessant stretching and folding of the fluid parcels that contain the scalar. Turbulence creates smaller and smaller scales, with molecular diffusion of the scalar finally bridging the smallest length scale λ_{B}. The Batchelor scale λ_{B} is defined as the smallest length scale at which gradients of the scalar can be sustained by the flow [1].

Nevertheless, visible to the eye are large coherent regions that contain almost unmixed scalar. It is the purpose of this article to quantify these regions, and to link their edges to structures that persist for long times in the turbulent *velocity* field. To make this possible, we have designed an experiment in which we move with the mean flow of a turbulent jet. The scalar concentration in a planar section is measured using laser-induced fluorescence (LIF), while the velocity field is measured using particle image velocimetry (PIV). The two cameras used for LIF and PIV, respectively, are traversed with a constant velocity, thus maximizing the time where turbulent structures remain in the observation window.

Large-scale structures of the scalar field—uniform concentration zones—are reminiscent of uniform *momentum* zones that are found in turbulent shear flows [2–4]. To identify these zones, we follow the elementary statistical approach of cluster analysis. The result of this procedure is a concentration field, coarsened into zones where the concentration is more or less constant. Cluster analysis, first introduced in the analysis of turbulent structures by [5], is a variation on the histogram method, which was first used by [2] to find velocity structures in the turbulent boundary layer.

---

[*]w.vandewater@tudelft.nl

Large-scale structures of the velocity field are characterized by finite-time Lyapunov exponents. The Lyapunov exponent $\Lambda_{\pm T}(\boldsymbol{x})$ gauges the exponential separation of fluid parcels at location $\boldsymbol{x}$, either in forward time (Λ_T) or backward time (Λ_{-T}). Ridges of local maxima of these scalar fields are known as Lagrangian coherent structures (LCS) [6]. In two-dimensional time-dependent chaotic flows, LCS play a role analogous to that of stable and unstable manifolds in time-*in* dependent chaotic fields, where they form inpenetrable barriers for scalar transport. In time-*dependent* two-dimensional flows, LCS form transient barriers of transport [6]. Lagrangian coherent structures have been demonstrated mainly in two-dimensional chaotic flows and two-dimensional turbulence. [7,8], and in effectively two-dimensional geophysical flows [9]. Twardos *et al.* [10] analyzed an experiment on a weakly turbulent two-dimensional flow, using the related concept of *stretching fields* [8]. Line-shaped maxima of the finite-time *past* Lyapunov field were found acting as barriers of scalar transport.

The purpose of our research is to associate the edges of uniform concentration zones with maxima of the scalar finite-time Lyapunov fields $\Lambda_{\pm T}(\boldsymbol{x})$. Turbulence generally arises from the instability of a main flow that carries the turbulent fluctuations away. This is true for turbulent boundary layers, for turbulent flow around obstacles, and for flow emanating from an orifice that becomes turbulent through shear instability. In all these cases turbulent flow structures are carried by the mean flow, and observing their evolution over a long enough time interval necessitates a moving observation window. We must move with the mean flow to adequately resolve the fine structure of the finite-time Lyapunov field. Lagrangian measurements of turbulent jets are not new; they have been used, for example, to track particles for two-point statistics [11], or to measure statistics near a turbulent-nonturbulent interface [12], but in all cases with a fixed camera frame which severely limits the observation time.

Our experiments involve a turbulent jet flow in water. The jet is seeded with tracer, whose concentration is measured using LIF. In snapshots of the concentration field we identify regions with more-or-less uniform concentration. We find the edges of these regions, which we correlate with maxima of the finite-time Lyapunov field. We follow two routes to establish this connection: conditional averages and the ordinary correlation function. In conditional averages [13], we compute the averaged field $\langle \Lambda_{\pm T}(\boldsymbol{x} - \boldsymbol{x}_0) \rangle$, with $\boldsymbol{x}_0$ the location of a concentration edge. If indeed ridges of $\Lambda_{\pm T}(\boldsymbol{x})$ coincide with edges of scalar zones, then the conditional average would be nonzero only at $\boldsymbol{x} = \boldsymbol{x}_0$.

In the next section we describe the experimental apparatus. The way to find uniform concentration zones is described in Sec. III, while the finite-time Lyapunov field $\Lambda_{\pm T}(\boldsymbol{x})$ is discussed in Sec. IV. The necessity of long observation times is illustrated in Sec. IV A. The correlation between the edges of uniform concentration zones and $\Lambda_{\pm T}(\boldsymbol{x})$ is quantified in Sec. V.

Lagrangian coherent structures became popular in the context of two-dimensional (geophysical) flows. The question is how to fruitfully apply this concept to scalar dispersion in fully developed three-dimensional turbulence.

II. EXPERIMENTS

The experiments involve a turbulent jet which is seeded with fluorescent dye. In a laboratory fixed frame (Eulerian frame), the observation of Lagrangian dynamics is limited by the passage of flow structures through the observation window. Therefore, an experiment was designed where the detection moves with the mean flow. Separate cameras were used for particle image velocimetry and laser induced fluorescence to measure the velocity- and concentration field in a thin slice of the evolving turbulent jet.

Figure 1 shows a schematic view of the experiment. The jet emanates from a 5 mm diameter orifice in a water tunnel (length 5 m, cross section $0.6 \times 0.6 \, \mathrm{m}^2$). The jet is fed from a constant-height reservoir, seeded with Rhodamine-B dye. The orifice-diameter-based Reynolds numbers are 5×10^3 and 10^4. The diffusivity of the dye is $4.5 \times 10^{-10} \, \mathrm{m}^2 \, \mathrm{s}^{-1}$, so that the Batchelor scale is
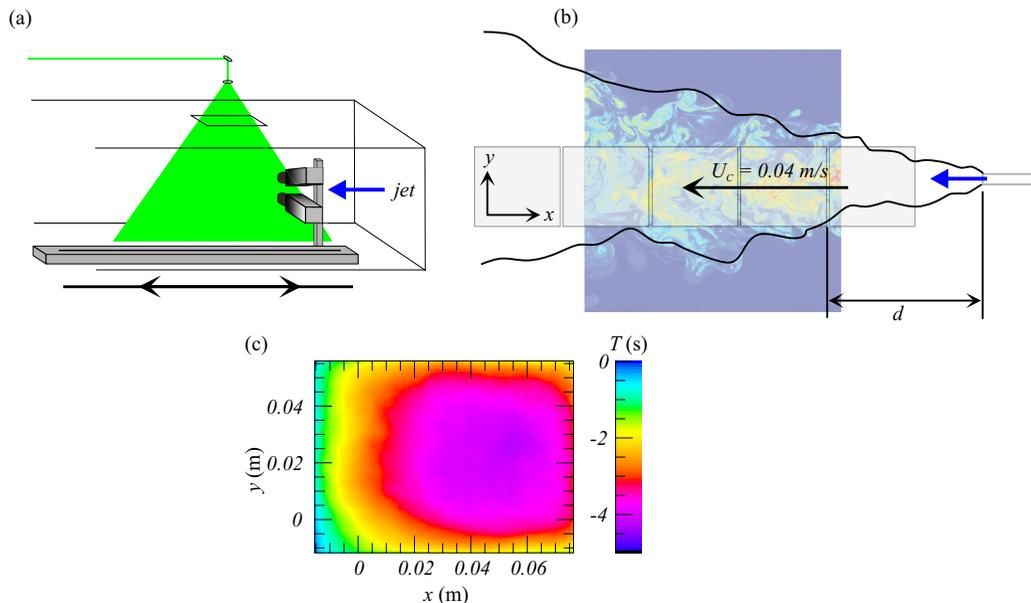
FIG. 1. The experimental setup. (a) Schematic view of the arrangement of cameras, traversing system and jet (not to scale). (b) Schematic view of the turbulent jet and sketch of the comoving observation window (not to scale). In a each run a total of 210 PIV frames and 101 LIF frames is acquired at a rate of 10 Hz. The coordinates within a comoving frame are (x, y), the distance of its right edge to the orifice is d. (c) Mean observation time in the comoving frame when integrating the separation of fluid parcels backwards in time. A maximum time of $|T| = 4$ s corresponds to a traveled distance of $d = 0.16$ m from the jet orifice. In a stationary Eulerian frame fluid structures move with the mean jet velocity. In this case they could only have been observed over 0.08 m for fluid parcels starting at the very right border of the frame (and 0.04 m for structures starting halfway).

$\lambda_B \approx 10^{-5}$ m, which is much smaller than a pixel (2.7×10^{-4} m). Consequently, the observed dye concentration field is caused by turbulent mixing only.

PIV and LIF measurements are done using two 16-bit, 5 Megapixel ScMos-cameras (LaVision), controlled by a PC using DAVIS 10 and equipped with a 105 mm focal length lens. The image acquisition frequency is 10 Hz. The PIV-camera is equipped with a shortpass filter (FES0550, Thorlabs, <550 nm) with a transmission ratio in the rejection region of 0.01%, while the LIF camera has a long-pass filter (FEL0550, Thorlabs, >550 nm) with a transmission ratio in the rejection region of 0.01%. Both the PIV- and LIF measurements are done using a double-pulsed Nd:YAG laser (Spectra Physics' Quanta Ray), with the laser beam formed into a 2-mm-thin laser sheet using (cylindrical) lenses. The light sheet is directed into the water through a plexiglas container, which eliminates perturbation of the laser sheet by the wavy air-water interface. Geometric calibrations are done using a calibration grid, while the concentration measurement was calibrated over the entire measurement range ($d = [0.36 \ldots 0.76$ m]) using a container with known dye concentrations. This also calibrates the intensity distribution in the laser sheet.

The 2-m-long traverse mechanism is driven by a stepper motor (MDrive 23 Hybrid, Schneider Electric, Marlborough, MA), which is synchronized to the images acquisition. A 0.8 m run up is used to reach constant velocity during a measurement, which ranges from 0.14 m to 0.98 m from the orifice. Using a random dot pattern, fixed to the side of the water tunnel, we have checked the velocity fluctuations of the traverse mechanism using PIV. At a nominal velocity of 4×10^{-2} m/s, the root-mean-square (rms) fluctuations are 5×10^{-4} ms/s. To allow for up to $T = 6.4$ s integration time for past- and future finite-time Lyapunov exponents, LIF images are collected between $d = 0.36$ and 0.76 m.

Statistics was collected over 20 repetitions of the experiment where the observation window moved from the near- to the far field of the jet, with a total of 210 velocity fields and 101 concentration fields in each run. We will only show the results of the $Re = 5 \times 10^3$ experiment; the correlation between zone edges and Lyapunov fields for the $Re = 10^4$ experiment was the same. The experimental setup is shown schematically in Fig. 1. Most relevant is the gain in observation time before turbulent structures exit the field of view in this Lagrangian setup. As Fig. 1(b) illustrates, this gain can be up to a factor of four compared to an Eulerian measurement.

III. UNIFORM CONCENTRATION ZONES

The zonal characterization of the concentration field was inspired by the recognition of uniform *momentum* zones in turbulent boundary layers [2–4]. To find uniform concentration zones we follow the well-established methods of cluster analysis [14], which were recently introduced in turbulence [5]. The starting point is the histogram $P_{his}(c)$ of concentrations c in a snapshot. In the case of n_{zones} clustered concentration values, which may still be spread over the observation window, this histogram is characterized by n_{zones} well-separated peaks. Each peak signifies a cluster, i.e., a uniform concentration zone. In practice, clusters are not so well defined and the art becomes to decompose the histogram into a sum of peaked distributions that are centered on n_{zones} distinct concentration values.

The histogram $P_{his}(c)$ is a discrete estimation of the underlying probability density function $P(c)$. The number of clusters is the number of local maxima of $P(c)$. A standard statistical procedure exists to overcome ambiguity associated with the width and placement of the discrete histogram bins [15]. The trick is to endow each pixel value with a Gaussian distribution of concentrations with width h, and sum them. A question is the choice of the smoothing factor h. It can be proven that for a Gaussian probability distribution function $P(c)$ the optimum h is $h = \alpha \, \sigma_P \, n^{-1/5}$, where σ_P is the standard deviation of $P(c)$ and $\alpha = 1.06$. Of course, in our case $P(c)$ is not a Gaussian (we are counting its local maxima), but experience teaches that this choice for h is adequate. It appears that a value $\alpha = 0.5$ severely overestimates the number of zones, while $\alpha = 1.5$ results in an underestimate.

Cluster analysis to find uniform concentration zones in each concentration snapshot can be compared to the *ad hoc* method for finding uniform *momentum* zones [2–4]. The cluster algorithm finds the optimum assignment of all local (pixel) concentration values to n_{zones} cluster values. The outcome, which is illustrated in Fig. 2(c), consists of n_{zones} component PDFs, which are not restricted to Gaussians, and which add up almost exactly to the measured PDF of measured concentrations in a snapshot. The cluster algorithm is preferred as it does not need chosen parameters or threshold values, apart from the number of zones. The first moments of these PDFs determine the concentrations in the coarsened field of Fig. 2(b). The KDE method applied to the data of Fig. 2(a) suggests a number of zones $n_{zones} = 4$, which was used as input to the cluster algorithm. Clearly, $n_{zones} = 3$ could have been another choice, however, using this in the cluster algorithm leaves the edge of the prominent zone at $c = 0.7$ in place.

A zonal characterization of the scalar field would be perfect if the PDF of the field consists of isolated peaks. However, as Fig. 2(c) also illustrates, the component PDFs overlap such that concentrations ascribed to one zone could also be member of another zone which is adjacent in concentration. Therefore, a measure of the degree of clustering is to compare the width of the component PDFs to the separation of peaks,

$$\text{Cl} = \frac{1}{n_{zones} - 1} \sum_{k=1}^{n_{zones}-1} 2 \frac{c_{k+1} - c_k}{w_{k+1} + w_k}, \tag{1}$$

with w_k the width at half maximum of a component PDF and c_k the first moment of the PDF of zone k. The contrast Cl increases with increasing peak separation and decreasing peak width.
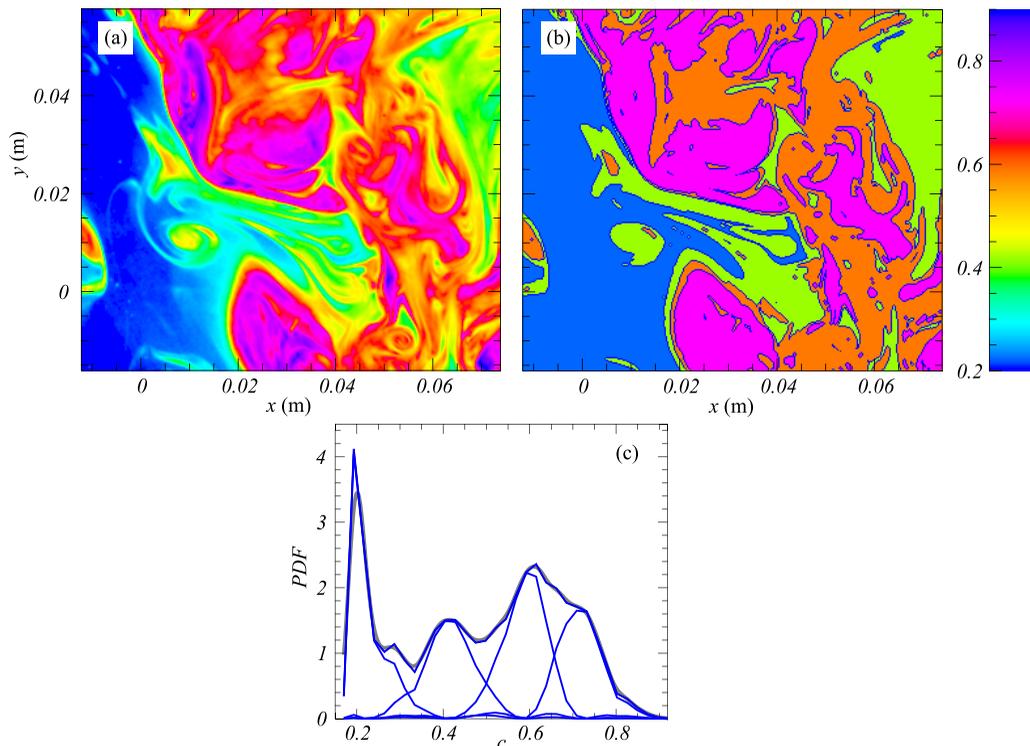
FIG. 2. (a) Snapshot of tracer concentration $c(\boldsymbol{x}, t)$, taken at $d = 0.83$ m from the jet orifice. (b) Field of panel (a), coarsened into four uniform concentration zones. (c) Finding uniform concentration zones. Blue lines: membership distribution of each of the four zones. Black line: sum of membership distributions, nearly coinciding with the histogram of concentrations in the field of frame (a). Gray line: smoothed histogram used in the kernel density estimate (KDE) of the number of zones ($n_{\mathrm{zones}} = 4$).

For the present experiment, the (dimensionless) Cl is shown in Fig. 3(a). It is compared to the contrast of uniform *momentum* zones in a turbulent boundary layer, using data from [4]. Indeed, the zonal characterization of the streamwise momentum in turbulent boundary layers [2] appears to be stronger than that of the concentration field in this experiment. Still, we believe that zones remain a viable concept in characterizing the organization of concentration in the jet.

An unbiased count of the number of zones in the evolving jet, averaged over 20 repetitions of the experiment, is shown in Fig. 3(b). The KDE method predicts an average $n_{\mathrm{zones}} = 4$, with an rms variation of 1. Consequently, we have fixed the number of zones to 4 throughout. The choice of n_{zones} affects the location of the zone edges. However, as is also argued by [5], a variation of 1 does not have a large influence on the most important edges. The evolution of the relative size of the zones is shown in Fig. 3(c). Downstream coarsening of the concentration field would imply that the large structures grow at the expense of smaller zones. No such coarsening is observed.

Apart from the large-scale structures, the cluster algorithm leaves small isolated patches. When computing correlations with the Lyapunov field, we have removed these patches if their relative area is $< 5 \times 10^{-3}$ of the full frame. Once the zones are identified, the zone edge field $I_e(\boldsymbol{x}, t)$ is constructed: $I_e(\boldsymbol{x}, t) = 1$ when $\boldsymbol{x}$ is on a zone edge, and zero otherwise.

The overall concentration PDF at our Reynolds numbers $\mathrm{Re} = 5 \times 10^3$ and $\mathrm{Re} = 10^4$ has a global maximum at finite concentration, and is otherwise characterized by local maxima that are associated with uniform concentration zones. A transition to a more thoroughly mixed state, as
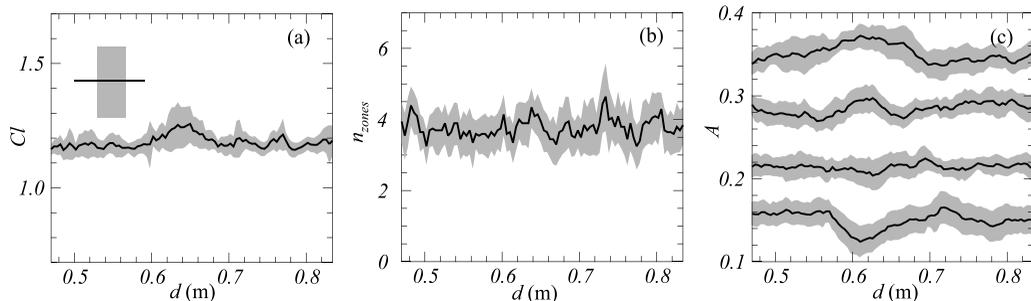
FIG. 3. (a) Degree of clustering Cl [see Eq. (1)] as a function of distance d to the jet orifice at $d = 0$. Full line: mean over 20 realizations, the width of the gray band is the rms fluctuation. A single point with error bar represents Cl for the clustering of the fluctuating streamwise velocity in a turbulent boundary layer [data of [4]]. (b) Kernel density estimate of the number of zones n_{zones} as a function of distance d. Full line: mean over 20 realizations, gray band: rms fluctuation. (c) Averaged area of zones as a function of d. The lines are ordered according to the area of a zone in each individual frame. No significant coarsening of the zones in the jet far field is observed.

characterized by a monotonic concentration PDF, was identified in [16] at slightly larger Reynolds numbers (Re $\gtrsim 2 \times 10^4$).

IV. FINITE-TIME LYAPUNOV FIELDS

Finite-time Lyapunov exponents gauge the exponentially fast spreading of nearby points, either for positive or negative times. They were computed from the measured velocity field $\boldsymbol{u}(\boldsymbol{x}, t)$ and strain field $\mathbf{A}(\boldsymbol{x}, t) = \nabla \boldsymbol{u}(\boldsymbol{x}, t)$ by integrating a separation vector $\boldsymbol{\delta}(t)$ along a Lagrangian trajectory,

$$\frac{d\boldsymbol{\delta}}{dt} = \mathbf{A}(\boldsymbol{x}(t), t) \cdot \boldsymbol{\delta}(t), \quad \text{with} \quad \frac{d\boldsymbol{x}(t)}{dt} = \boldsymbol{u}(\boldsymbol{x}, t). \tag{2}$$

The time integration of Eq. (2) over an interval t_0, t defines the evolution matrix $\mathbf{M}_{t_0}^t$ as $\boldsymbol{\delta}(t) = \mathbf{M}_{t_0}^t \cdot \boldsymbol{\delta}(t_0)$. This matrix was computed for each grid point as initial position $\boldsymbol{x}_0$. For convenience, the two initial separation vectors $\boldsymbol{\delta}(t_0)$ are chosen along the coordinate axes. The quality of the PIV data warrants the integration of Eq. (2) using the strain field $\mathbf{A}$, a procedure which is superior to computing $\mathbf{M}_{t_0}^t$ by following fluid parcels. The integration of Eq. (2) was done using a simple forward Euler scheme, and the velocity and strain fields at $\boldsymbol{x}(t)$ were computed from the measured data using bilinear interpolation.

The largest eigenvalue λ_2 of the positive Cauchy-Green tensor,

$$\mathbf{C}_{t_0}^t = \mathbf{M}_{t_0}^t \left(\mathbf{M}_{t_0}^t \right)^{\dagger}, \tag{3}$$

with $\dagger$ the adjoint, then defines the finite-time *future* Lyapunov exponent Λ_T as

$$\Lambda_{t_0}^{t_0+T}(\boldsymbol{x}_0) = \frac{1}{2T} \ln(\lambda_2). \tag{4}$$

Similarly, by integrating the trajectories *backward* in time, the largest eigenvalue of $\mathbf{C}_{t_0}^{t_0-T}$ defines the *past* Lyapunov field $\Lambda_{t_0}^{t_0-T}(\boldsymbol{x}_0)$.[1] In a stationary two-dimensional flow, local maxima of $\Lambda_{\pm T}$ form invariant lines that are inpenetrable for scalar transport. In a time-dependent flow, these local maxima are expected to still organize scalar transport. This was proved for local maximum ridges of the Lyapunov field by [6]. Alternatively, [8,17] emphasize the role of of lines of least stretching as

---

[1]Throughout we use the shorthand Λ_T for $\Lambda_{t_0}^{t_0+T}$ and Λ_{-T} for $\Lambda_{t_0}^{t_0-T}$.
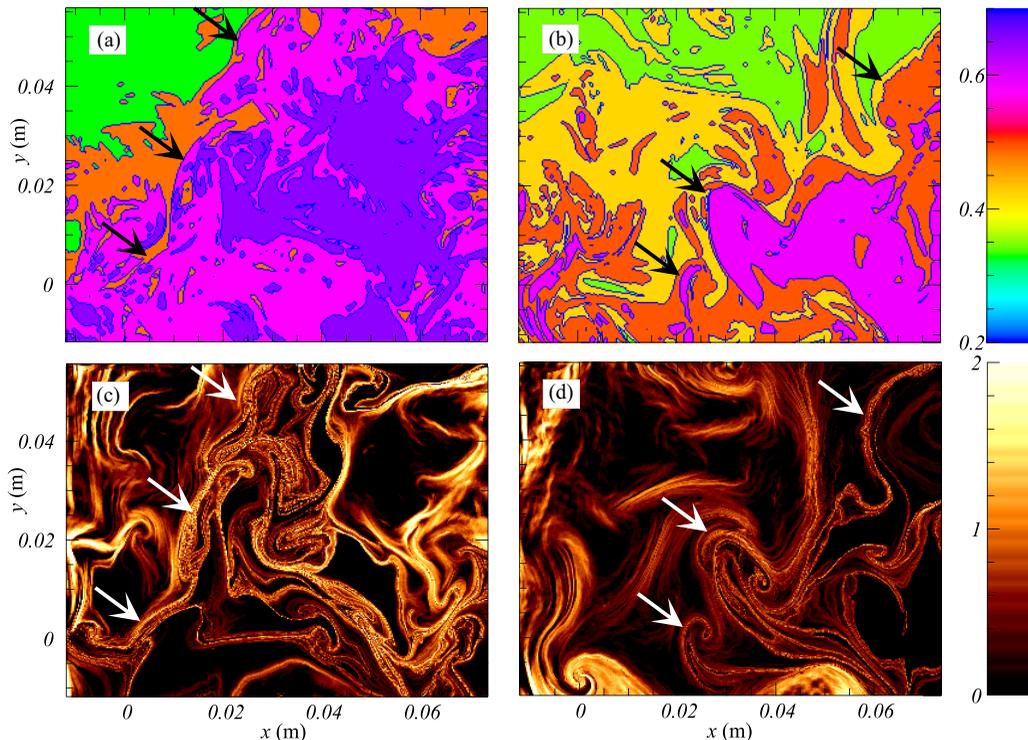
FIG. 4. Comparison of backward-time Lyapunov field (c), (d) Λ_{-T} to the concentration field (a), (b) in two snapshots of a single scan, which also illustrates the temporal evolution of the fields. (a), (c) At $d = 0.67$ m, (c), (d) at $d = 0.83$ m. The large-scale filamentous structure of $\Lambda_{-T}(\boldsymbol{x})$ roughly corresponds to the large-scale structure of the edges of the uniform concentration zones (suggested by arrows).

transport barriers in 2D flows. The eigenvalues and eigenvectors of $\mathbf{C}_t^{t+T}$ are advected by the flow. However, as time progresses, the flow field dynamically evolves and $\mathbf{C}_t^{t+T}$ evolves accordingly. The question is at what time t' should the scalar zone edge field $I_e(\boldsymbol{x}, t')$ be compared to structures of $\mathbf{C}_t^{t+T}$ or $\mathbf{C}_t^{t-T}$: should t' be chosen t or a later or earlier time?

Two snapshots of $\Lambda_{-T}(\boldsymbol{x})$ are shown in Fig. 4. They display remarkable detail. The long integration time in our genuine Lagrangian experiment makes the filamentous structure of $\Lambda_{-T}(\boldsymbol{x})$ stand out very clearly. The claim is that, among those structures, the local maximum ones are central in the organization of scalar transport. Procedures to extract those maximum ridges have been described by [6], while the refinement of ridges of $\Lambda_{\pm T}$ to transport barriers was detailed in [18,19]. Their approach involves a quest for local maxima among candidate curves.

The Lyapunov fields are shown together with the corresponding coarsened concentration fields in Fig. 4. Visible to the eye are structures that occur in both fields. Those have been marked. The frames are mere snapshots selected from a single run. The challenge is to quantify the correspondence between the fields statistically in averages over many runs.

In this paper we will investigate the relation between $\Lambda_{\pm T}(\boldsymbol{x})$ and the scalar concentration edges, emphasizing local maxima of $\Lambda_{\pm T}$ by only including points where $\Lambda_{\pm T}$ is convex in the direction of the eigenvector $\boldsymbol{\xi}_2$ corresponding to the largest eigenvalue λ_2 of $\mathbf{C}_t^{t\pm T}$, $\boldsymbol{\xi}_2 \cdot \mathbf{H} \cdot \boldsymbol{\xi}_2 < 0$, with the Hessian $\mathbf{H}_{ij} = \partial^2 \Lambda_{\pm T}(\boldsymbol{x})/\partial x_i \partial x_j$. We further restrict $\Lambda_{\pm T}$ to positive values and highlight maxima of $\Lambda_{\pm T}$ by computing conditional averages using its square $\Lambda_{\pm T}^2$. Concluding, we perform only part of the refinements by [18], but we expect that this will not affect the correlation with the scalar field qualitatively.
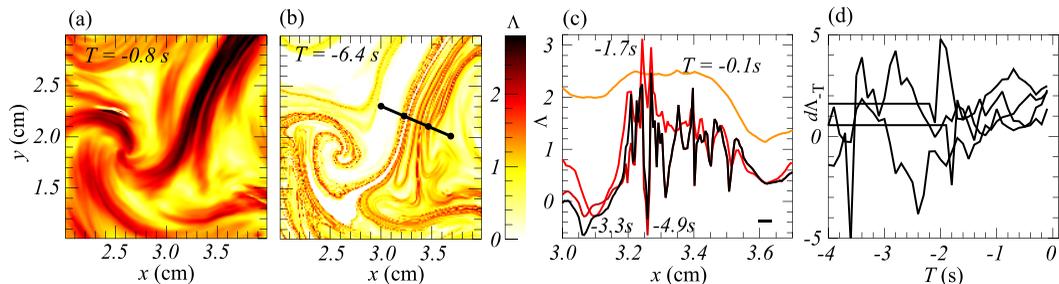
FIG. 5. Evolution with integration time T of the time-backward finite-time Lyapunov field Λ_{-T} in the Lagrangian frame. (a) After $T = 0.8$ s, (b) after 6.4 s. (c) Evolution of Λ_{-T} on the line in (b) which intersects a filament. At increasing integration time, $T = 0.1$, 1.7, 3.3, and 4.9 s, structures with increasing detail emerge. The bar indicates the Kolmogorov scale. (d) The evolution of increments $d\Lambda_{-T}$ measured at the 4 intersection points shown in panel (b). The two points with largest x have already left the observation window at $T \approx 2$ s.

Before discussing the correlation between $\Lambda_{\pm T}(\boldsymbol{x})$ and the instantaneous zone edges $I_e(\boldsymbol{x})$, we will first quantify the emergence of fine-scale structure of $\Lambda_{-T}(\boldsymbol{x})$ with increasing integration time T.

A. Evolution of Λ_{-T}

Figure 5 shows the evolution of the backward-time $\Lambda_{-T}(\boldsymbol{x})$ with increasing integration time. Most detail emerges at the longest integration time, $T = 6.4$ s. For some regions in Fig. 5(b), fluid parcels have already left our comoving frame at shorter integration times. The evolution $\Lambda_{-T}(\boldsymbol{x})$ on a line $\boldsymbol{x}(s)$ of initial conditions is shown in Figs. 5(c) and 5(d). Increasingly fine-scale structure appears for increasing integration time T, which illustrates the necessity of measuring turbulence in a frame moving with the mean velocity. For some regions $\boldsymbol{x}(s)$, the integration time is limited by the disappearance of flow structures from our comoving field of view.

Figure 5(d) shows the increments $d\Lambda_{-T_i} = i\Lambda_{-T_i} - (i-1)\Lambda_{-T_{i-1}}$ at times $T_i = i\,dT$, with $dT = 0.1$ s for 4 points along the section $\boldsymbol{x}(s)$. These increments are analogous to finite-time Lyapunov exponents measured over time intervals of length 0.1 s; the time-average of $d\Lambda_{-T_i}$ is Λ_{-T}. The short-time $d\Lambda_{-T_i}$ are strongly fluctuating, and there is an interesting connection with the theory of chaotic dynamical systems [20]. Two of the points on $\boldsymbol{x}(s)$ have already left the observation window at ≈ 2 s.

In an experiment scan of the observation window, the distance d to the jet orifice ranges from $d = 0.40$ m to $d = 0.76$ m, and the turbulence characteristics change approximately by a factor 2. Taking the median integral length scale $L \approx 0.05$ m, and the median turbulent fluctuation velocity $u \approx 0.012$ m/s, gives a large-eddy turnover time $\tau_L \approx 4$ s. This is also the time scale on which fine structure of Λ_{-T} is created.

In analogy to the Lagrangian structure of a passive scalar field [21], we hypothesize that the structure of $\Lambda_{\pm T}$ is due to the concentration of small-scale gradients by the Lagrangian field *itself*. The smallest scales l are determined by the balance between the concentration of gradients and diffusion of momentum ν, $l \propto (\nu/\Lambda_{-T})^{1/2}$ [22]. For our experiments, $l \approx 6 \times 10^{-4}$ m, which is comparable to the Kolmogorov scale in the region of interest $\eta \approx 4 \times 10^{-4}$ m. Surprisingly, the velocity field creates significantly smaller structures of $\Lambda_{-T}(\boldsymbol{x})$.

V. CORRELATIONS

By its very nature, the finite-time Lyapunov field is thought to organize the distribution of scalar concentration [6,8]. The present experiment gives access to both fields. We have reduced the concentration field to edges of uniform concentration zones, and have designed our experiment
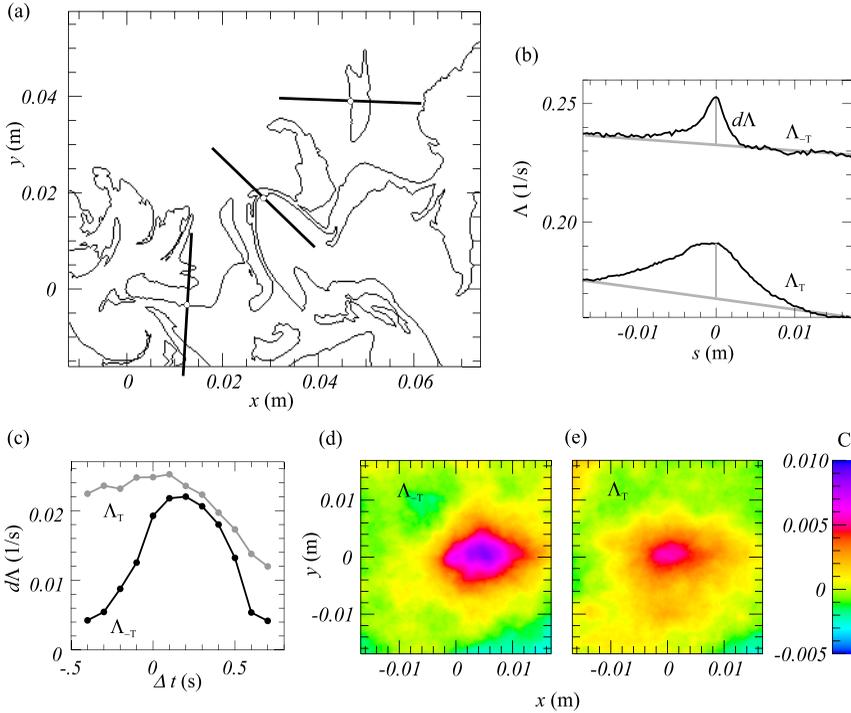
FIG. 6. Relation between the finite time Lyapunov field $\Lambda_{\pm T}$ and the edges of uniform concentration zones. (a) Illustration of conditional averages on lines perpendicular to zone edges. Three of these lines $\boldsymbol{n}(s)$ are shown, the corresponding zone edge at $s = 0$ is indicated by the circle. In comparison to Fig. 4, small zones with a relative area of 10^{-3} have been removed. (b) Perpendicular conditional averages of $\Lambda_{\pm T}$. Only the past Lyapunov field Λ_{-T} shows a well-defined peak at zone edges I_e. (c) Dots conected by lines: height of the peak in Λ_{-T} above the background [as illustrated in (b)] as a function of the delay between Λ_{-T} and the zone edge field I_e, gray line: same for the peak in Λ_T. (d, e) Normalized correlation $C(\boldsymbol{r})$ between edges and the Lyapunov fields $\Lambda_{\pm T}$. It is defined as $C(\boldsymbol{r}) = \langle \Lambda_{\pm T}(\boldsymbol{x} + \boldsymbol{r}) \, I_e(\boldsymbol{x}) \rangle_{\boldsymbol{x},t,r}$, where $I_e(\boldsymbol{x})$ is the zone edge field: $I_e(\boldsymbol{x}) = 1$ when $\boldsymbol{x}$ is on an edge, and zero otherwise.

such that the sharp structures of the Lyapunov $\Lambda_{\pm T}$ field can be resolved. In finding a connection between the edges of uniform scalar concentration and regions of large $\Lambda_{\pm T}$ we follow two avenues: conditional averaging and the simple planar correlation between the two fields.

The conditional average is done by computing $\langle \Lambda_{\pm T}(\boldsymbol{n}, t) \rangle_{\boldsymbol{n},t,r}$, along $\boldsymbol{n}(s)$ with $\boldsymbol{n}$ a vector perpendicular to a zone edge with the edge at $\boldsymbol{n} = 0, s = 0$. Three of these lines $\boldsymbol{n}(s)$ are shown in Fig. 6(a). Averages are done over a fraction of the discrete edge points of a zone ($10^2 \ldots 10^3$ points), over 100 snapshots t in a single scan, and over $r = 20$ runs. By varying the number of runs we have checked statistical convergence. In computing conditional averages and correlations, a restriction was made to part of the interval $x = [0, 0.07 \text{ m}]$ (see Fig. 4) where the average observation time $|T| \gtrsim 4$ s.

If edges would correspond to local maxima of $\Lambda_{\pm T}(\boldsymbol{x})$, then a conditional average would single out this maximum value at $s = 0$ and $\langle \Lambda_{\pm T}(\boldsymbol{n}, t) \rangle_{\boldsymbol{n},t,r}$ would sharply peak at $s = 0$. If the correspondence is exact, then there would be no accidental conditional average outside this peak, which would then reside on a zero background. However, as is clear from Fig. 6(a), lines $\boldsymbol{n}$ can cross several edges and a nonzero background is expected. The conditional averages of Λ_{-T} and Λ_T are shown in Fig. 6(b). That of Λ_{-T} displays a clear preference for the edges of uniform concentration zones while Λ_T is not correlated strongly with edges. In both cases there is a large background.

An interesting question is if the correlation of the edge field $I_e(\boldsymbol{x}, t)$ and Λ_t^{t-T}, Λ_t^{t+T} occurs at the same time t. As Fig. 6(c) illustrates, the maximum conditional average between the edge field $I_e(\boldsymbol{x}, t')$ and the backward time Lyapunov Λ_t^{t-T} field occurs at a time $t' = t - \Delta t$, with the concentration edge field delayed by $\Delta t \approx 0.2$ s. No such marked time dependence is found for the forward time Lyapunov field Λ_t^{t+T}, in agreement with the much weaker spatial selectivity.

Conditional averaging is a way to express the significance of an edge for the scalar Lyapunov field. If, instead, the Lyapunov field could be reduced to lines (for example to Lagrangian Coherent Structures), then the relation of these lines to sharp gradients in the concentration field could be investigated.

The ordinary correlation $C(\boldsymbol{r})$ between the edge field $I_e(\boldsymbol{x}, t)$ and $\Lambda_{-T}(\boldsymbol{x})$ is shown in Fig. 6(d) and that of Λ_T in Fig. 6(e). The correlation is defined as $C(\boldsymbol{r}) = \langle \Lambda_{\pm T}(\boldsymbol{x} + \boldsymbol{r}) I_e(\boldsymbol{x}, t) \rangle_{\boldsymbol{x}, t, r}$. The correlation function $C(\boldsymbol{r})$ is normalized such that $C = 1$ signifies perfect correlation and $C = 0$ is complete absence of correlation. Clearly, Λ_{-T} is correlated more strongly with the edge field than Λ_T, with a maximum value $C \approx 10^{-2}$. We conclude that conditional averages are a better probe for the relation between the Lyapunov- and zone edge fields than the ordinary correlation functions.

VI. CONCLUSION

By observing large-scale coherent structures of a velocity field one may be able to predict the spreading of pollutant without having to solve the detailed velocity field. Locations where the spreading of closely spaced fluid parcels is maximal may form the structures sought for. It is our purpose to find this connection in an experiment.

Although the structure of the finite-time Lyapunov field $\Lambda_{-T}(\boldsymbol{x})$ resembles that of the edge field of scalar zones, they do not coincide. There is structure of $\Lambda_{-T}(\boldsymbol{x})$ inside a concentration zone, and there are edges where no maximum line of $\Lambda_{-T}(\boldsymbol{x})$ exists. This is reflected quantitatively in either the plain correlation function or the conditional average of $\Lambda_{-T}(\boldsymbol{x})$ on edges of concentration zones.

The enhancement of the conditional average on edges is small (≈ 0.02). Consistently, however, edges correspond to large *backward* time Lyapunov exponents $\Lambda_{-T}(\boldsymbol{x})$, and not to *forward* time $\Lambda_T(\boldsymbol{x})$ ones. Thus, edges of uniform concentration zones correspond to *stable* manifolds that *attract* fluid parcels in forward time. The fields $\Lambda_t^{t-T}(\boldsymbol{x})$ and $I_e(\boldsymbol{x}, t')$ where a maximum conditional average is found are nearly synchronous ($t' = t - 0.2$ s). This is remarkable since Λ_t^{t-T} embodies information of the velocity field and its gradients over the previous $T \approx 6.4$ s.

There are several reasons why the found connection is not strong. First, we take a two-dimensional slice out of a three-dimensional velocity field. Second, despite our experimental effort to move with the flow, our observation time is still limited to one large-eddy turnover time. Third, due to crowding of edges [see Fig. 6(c)], there is a large background of the conditional averages.

ACKNOWLEDGMENTS

---

[1] W. J. Dahm and P. E. Dimotakis, Mixing at large Schmidt number in the self-similar far field of turbulent jets, J. Fluid Mech. **217**, 299 (1990).

[2] R. J. Adrian, C. D. Meinhart, and C. D. Tomkins, Vortex organization in the outer region of the turbulent boundary layer, J. Fluid Mech. **422**, 1 (2000).

[3] C. M. de Silva, N. Hutchins, and I. Marusic, Uniform momentum zones in turbulent boundary layers, J. Fluid Mech. **786**, 309 (2016).

[4] J. Eisma, J. Westerweel, G. Ooms, and G. E. Elsinga, Interfaces and internal layers in a turbulent boundary layer, Phys. Fluids **27**, 055103 (2015).

[5] D. S. Fan, J. L. Xu, M. X. Yao, and J. P. Hickey, On the detection of internal interfacial layers in turbulent flows, J. Fluid Mech. **872**, 198 (2019).

[6] S. C. Shadden, F. Lekien, and J. E. Marsden, Definition and properties of Lagrangian coherent structures from finite-time Lyapunov exponents in two-dimensional aperiodic flows, Physica D **212**, 271 (2005).

[7] G. Haller and G. Yuan, Lagrangian coherent structures and mixing in two-dimensional turbulence, Physica D **147**, 352 (2000).

[8] G. Haller, Lagrangian coherent structures, Annu. Rev. Fluid Mech. **47**, 137 (2015).

[9] J. H. Bettencourt, C. Lopez, and E. Hernandez-Garcia, Oceanic three-dimensional lagrangian coherent structures: A study of a mesoscale eddy in the Benguela upwelling region, Ocean Model. **51**, 73 (2012).

[10] M. J. Twardos, P. E. Arratia, M. K. Rivera, G. A. Voth, J. P. Gollub, and R. E. Ecke, Stretching fields and mixing near the transition to nonperiodic two-dimensional flow, Phys. Rev. E **77**, 056315 (2008).

[11] B. Viggiano, T. Basset, S. Solovitz, T. Barois, M. Gibert, N. Mordant, L. Chevillard, R. Volk, M. Bourgoin, and R. B. Cal, Lagrangian diffusion properties of a free shear turbulent jet, J. Fluid Mech. **918**, A25 (2021).

[12] R. R. Taveira, J. S. Diogo, D. C. Lopes, and C. B. da Silva, Lagrangian statistics across the turbulent-nonturbulent interface in a turbulent plane jet, Phys. Rev. E **88**, 043001 (2013).

[13] D. K. Bisset, J. C. R. Hunt, and M. M. Rogers, The turbulent/nonturbulent interface bounding a far wake, J. Fluid Mech. **451**, 383 (2002).

[14] J. C. Bezdek, A convergence theorem for the fuzzy ISODATA clustering algorithms, in *IEEE Transactions on Pattern Analysis and Machine Intelligence*, Vol. PAMI-2 (IEEE, Piscataway, NJ, 1980), pp. 1–8.

[15] B. W. Silverman, *Density Estimation for Statistics and Data Analysis*, Monographs on Statistics and Applied Probability (Chapman and Hall, London/New York, 1986), p. 175.

[16] P. E. Dimotakis, The mixing transition in turbulent flows, J. Fluid Mech. **409**, 69 (2000).

[17] G. Haller and F. J. Beron-Vera, Geodesic transport barriers in two-dimensional flows, Physica D **241**, 1680 (2012).

[18] M. Farazmand and G. Haller, Computing Lagrangian coherent structures from their variational theory, Chaos **22**, 013128 (2012).

[19] Z. Wilson, M. Tutkun, and R. Cal, Identification of Lagrangian coherent structures in a turbulent boundary layer, J. Fluid Mech. **728**, 396 (2013).

[20] T. Bohr, M. H. Jensen, G. Paladin, and A. Vulpiani, *Dynamical Systems Approach to Turbulence*, Cambridge Nonlinear Science Series 7 (Cambridge University Press, Cambridge, UK, 1998), p. 301.

[21] D. Kushnir, J. E. Schumacher, and A. Brandt, Geometry of Intense Scalar Dissipation Events in Turbulence, Phys. Rev. Lett. **97**, 124502 (2006).

[22] E. Balkovsky and A. Fouxon, Universal long-time properties of lagrangian statistics in the Batchelor regime and their application to the passive scalar problem, Phys. Rev. E **60**, 4164 (1999).